RESEARCH ARTICLE | MAY 07 2024

Impact of drops of epoxy resin and hardener, silicone and turpentine oils onto balsa wood and polypropylene substrates

Rafael Granda ; Vitaliy Yurkiv ; Farzad Mashayek ; Alexander L. Yarin

Physics of Fluids 36, 053312 (2024)
https://doi.org/10.1063/5.0208144

Physics of Fluids ARTICLE pubs.aip.org/aip/pof

Impact of drops of epoxy resin and hardener, silicone and turpentine oils onto balsa wood and polypropylene substrates

Cite as: Phys. Fluids **36**, 053312 (2024); doi: 10.1063/5.0208144
Submitted: 13 March 2024 · Accepted: 18 April 2024 ·
Published Online: 7 May 2024

Rafael Granda,[1] Vitaliy Yurkiv,[2] Farzad Mashayek,[2] and Alexander L. Yarin[1,a)]

AFFILIATIONS

[1]Department of Mechanical and Industrial Engineering, University of Illinois at Chicago, 842 W. Taylor St., Chicago, Illinois 60607-7022, USA
[2]Department of Aerospace and Mechanical Engineering, University of Arizona, 1130 N. Mountain Ave., Tucson, Arizona 85721, USA

[a)]**Author to whom correspondence should be addressed:** ayarin@uic.edu. **Tel.:** (312) 996-3472. **Fax:** (312) 413-0447

ABSTRACT

Electrowetting and wettability-driven spreading of liquids on porous and nonporous substrates was investigated using impact of drops of epoxy resin, epoxy hardener, and epoxy resin and hardener, as well as silicone and turpentine oils with oil-soluble aniline dyes onto balsa wood and polypropylene surfaces. The experimental results revealed that the electric field stretched drops of epoxy resin, epoxy hardener, and epoxy resin and hardener after impact on polypropylene substrate in the long-term. The spreading of drops of epoxy resin and turpentine oil with dyes after impact onto porous balsa wood under the action of a 10 kV applied voltage was relatively weak. In addition, the measured footprint areas corresponding to drops of epoxy resin, epoxy hardener, and epoxy resin and hardener demonstrated a significant increase in the wetted areas driven by the applied voltage of 10 kV on polypropylene substrate, whereas on balsa wood, the footprint is practically unaffected by the electric field. Furthermore, it was determined that surface wettability was the main mechanism of spreading of epoxy resin, as well as silicone and turpentine oils with aniline dyes on porous balsa without the electric field applied. On the other hand, insufficient concentration of ions and counterions in silicone oil was responsible for the absence of electrohydrodynamic effects after impact of such drops onto porous balsa substrate subjected to high potentials of 7 and 10 kV. Hence, wettability-driven spreading with imbibition on balsa wood was the only reason for an increase in the wetted area in the case of silicone oil.

I. INTRODUCTION

The dynamics of impact of drops of pure and mixed liquids of different chemical, electrical, and fluid properties onto dielectric solid surfaces has been investigated recently driven by important industrial applications. The experimental results on the impact of pure aqueous drops onto different types of dielectric substrates such as polypropylene, parafilm, and Teflon demonstrate that the application of an in-plane electric field affects the drop dynamics. For example, the resulting electric force partially or completely suppresses splashing and drop rebound, especially at highest electric field strengths (Lee *et al.*, 2013; Sankaran *et al.*, 2021; Yarin *et al.*, 2017; and Yurkiv *et al.*, 2018). Impacts of drops of suspensions of pigment particles, such as paints, have also been studied using dielectric intact surfaces without and with applied voltage acting in the substrate plane. In these cases, hydrodynamic behavior after drop impact was rather peculiar. It should be emphasized that paints are colloidal suspensions comprising several different types of solvents and pigment particles (Bochkarev *et al.*, 2011; Chen and Bonaccurso, 2014; Granda *et al.*, 2021b; Mugele and Baret, 2005; and Mugele and Heikenfeld, 2019). Accordingly, common solvents such as water, turpentine, and silicone oils mixed with water-soluble and oil-soluble aniline dyes, and titanium dioxide particles reveal fingerlike structures at different applied voltages, an increase in the painted area compared to the cases without voltage applied and significant drop stretching along the field lines (Granda *et al.*, 2021b; Granda *et al.*, 2022a; and Mikkelsen *et al.*, 2018).

Nevertheless, very few studies had in focus their impacts and spreading of drops of different solvents on porous substrates commonly used in our everyday life, such as wood. Experimental and numerical results revealed that drop behavior after impact onto balsa wood surfaces is less affected by the application of an in-plane electric field compared to the cases where no voltage was applied to such porous substrates. In particular, the experimental data revealed a

greater number of fingerlike structures developing along the drop rim (in the short-term, a few milliseconds after impact) under the action of the in-plane electric field. On the other hand, the wettability-driven spreading in the long term had a more significant effect than the effect of the electric field acting on the porous substrate. Therefore, the applied voltage presumably stretched only the diminishing upper part of such drops, which was still above the porous surface, that is, still was not imbibed (Granda *et al.*, 2022b; Yarin *et al.*, 2019). It is worth noting that the absorption of water in porous wooden materials could eventually affect the drop dynamics, as well as the properties of the substrates as well. Thus, the moisture content in wood strongly influences the properties of wooden materials (Fu *et al.*, 2019).

Furthermore, the relationship between the dynamics of wetting and the chemical composition of the surface has led to further research of this topic for different wood specimens. The results in Wang *et al.* (2015) indicated that thermal modification was capable of decreasing the dynamic wettability of wood by lowering the spreading speed and penetration rate of water drops into wood surfaces. When a drop spreads over the surface of a porous material, the contact line motion on the textured surface and capillary imbibition into the bulk of porous substrate determine the drop evolution. In addition, experimental and analytical results have demonstrated that drop evolution is influenced by the factors arising from capillary imbibition in porous media. For example, a lower porosity leads to a faster drop spreading, which in turn results in a decrease in the drop height (Frank and Perré, 2012). Similarly, studies on the mechanisms responsible for wetting and capillary imbibition of fluids such as water and silicone oil revealed that the apparent contact angle strongly depends on surface wettability and morphological characteristics of wood materials, including hardwood. In addition, surface wettability of different types of wood was strongly influenced by the thickness of the embedded fibers and surface roughness (Alia-Syahirah *et al.*, 2019; Benkreif *et al.*, 2021; and Zhou *et al.*, 2018).

Due to its hygroscopicity and permeability, wood has the ability to absorb, conduct, and lose water under different conditions. Hence, analytical and numerical attempts to elucidate the complexity of the porous surface-liquid interaction in wood have revealed that the validity of Young's equation is limited to homogeneous flat intact surfaces (which do not adsorb liquid). The inapplicability of Young's equation stems from the fact that wood is hydrophilic, anisotropic, and heterogeneous. For instance, the apparent contact angle changes over time which implies problems in determining equilibrium when analytical approaches are employed. Furthermore, numerical methods have confirmed that liquid absorption in the porous media in addition to spreading on the wood surface strongly determines the height of the liquid drop on the porous surface and the footprint of the wetted area at the spreading stage (Csanády *et al.*, 2015; Karniadakis *et al.*, 2005; Lee *et al.*, 2016; and Meng *et al.*, 2014). It should be emphasized that these investigations mainly utilized drops of water and oil and revealed that as soon as the drop made contact with the wood surface, it rapidly penetrated and spread out in the wood capillaries resulting in an extremely fast absorption of water and oil without application of external (e.g., electric) forces (Vidiella del Blanco *et al.*, 2017). Also, despite extensive research of drop dynamics on dielectric and nanotextured surfaces (Yarin *et al.*, 2014), there is a limited number of works on electrowetting and spreading phenomena on wood substrates.

The present study explores the electrically driven spreading of drops of pure epoxy resin, epoxy hardener, and epoxy resin and hardener, as well as silicone and turpentine oils with aniline dyes on porous and intact dielectric surfaces of balsa wood and polypropylene, respectively. Using these different materials allows us to evaluate the influence of morphological characteristics of the surface, its roughness, and surface wettability for the two above-mentioned widely used porous and nonporous substrates. The choice of the working fluids is determined by their extensive use and applications in industry. The different fluid and electrical properties, as well as the chemical structure and the origin of epoxy resin and hardener, as well as silicone and turpentine oils are all relevant in such a detailed investigation aiming at increasing surface coverage with less liquid being used. This study also aims an electrostatic facilitation of drop spreading on dielectric substrates. Accordingly, the experimental observations reveal that drops of epoxy resin and epoxy hardener experience a significant increase in drop stretching on polypropylene substrates when a DC voltage is applied to create an in-plane electric field. On the other hand, wettability-driven spreading of epoxy resin and turpentine oils with dyes competing with the electric-field spreading is evident on balsa wood. Additionally, the high-speed recordings reveal slight capillary impregnation of silicone oil drops into balsa, while the effect of the applied electric field is negligible in this case. Accordingly, silicone oil spreading over balsa wood is wettability-driven and is guided by grooves on balsa surface. In addition, this study demonstrates that a sufficient polarization of such porous and non-porous substrates can potentially be achieved with several other dielectric materials by applying an in-plane electric field. The non-aqueous liquids employed here without and with pigment particles also elucidate whether drop stretching of a specific pure liquid or a colloidal suspension could benefit from the application of DC voltages. Accordingly, the present work significantly extends and encompasses the results of Granda *et al.* (2022b).

In Sec. II, the experimental setup is described. Then, in Sec. III, the experimental findings and discussion are presented. Conclusions are drawn in Sec. IV.

II. EXPERIMENTAL SETUP AND MATERIALS

The experimental setup is sketched in Fig. 1. Balsa wood and polypropylene were used as the dielectric substrates in the present experiments. Balsa and polypropylene were carefully cut into 2 cm (length) × 2 cm (width) pieces with the thickness of 1.5 and 0.051 mm, respectively, with each of them being placed above two-plane electrodes made of a copper tape. Balsa wood (Bright Creations Balsa Wood Sheets) and polypropylene membrane (#7524T11) were obtained from Walmart and McMaster-Carr, respectively. The wooden and polypropylene surfaces used for the drop impact experiments were in the areas between the electrodes. The distance between the electrodes was kept constant at 1.5 cm in all the experiments conducted without and with the applied voltage. Outside of the electrodes, the balsa wood and polypropylene substrates were insulated by Teflon. The balsa and polypropylene substrates with electrodes and Teflon insulation were stuck on a microscope glass slide. One of the electrodes was connected to a positive high voltage supply (Glassman High Voltage Inc., EL40P1, custom built with a 0–20 kV range). The other copper electrode was grounded.

The glass slide with the balsa wood or polypropylene substrate equipped with the electrodes was mounted on the adjustable platform, which could be controlled in three directions, in particular, changing the height between the tip of the needle and the dielectric surface (cf. Fig. 1). Additionally, a fine-tune control along one of the horizontal

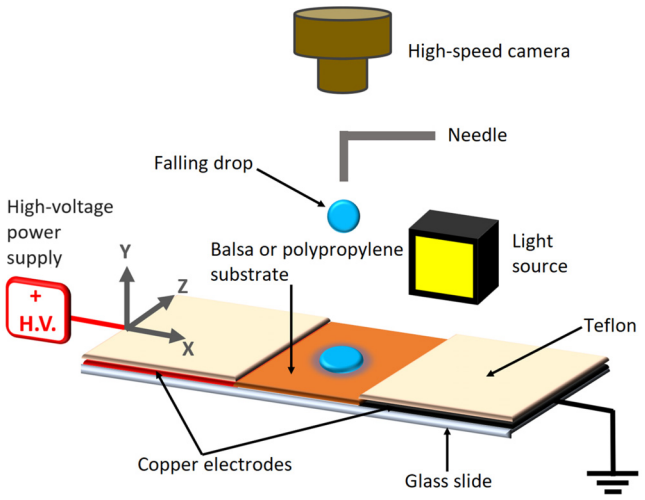

FIG. 1. Schematic of the experimental setup used to observe drop impact and spreading.

axes allowed one to aim the drop impact point at the inter-electrode center. In the present case, a nozzle height of 12.5 cm was kept constant throughout the experiments without and with the electric field. Additional experiments were conducted using only polypropylene substrate as the dielectric surface.

Epoxy resin, epoxy hardener, a mixture of epoxy resin and hardener (1:1 ratio), silicone oil, turpentine oil mixed with oil-soluble golden yellow oak aniline dye (7 wt. % concentration), and turpentine oil mixed with oil-soluble black aniline dye (10 wt. % concentration) were used as the working fluids in the present work. Epoxy resin and hardener (Epoxy Resin Clear Crystal Coating Kit), turpentine oil (Natural Pure Gum Spirits of Turpentine), and silicone oil (General purpose silicone fluid) were acquired from Amazon and Ametek Brookfield, respectively. A laboratory syringe pump (NE-1000 Series) delivered a working fluid to a 90°-bent 27-gauge needle at a flow rate of 2 ml/h for all the solvents used. The out-of-focus 90°-bent 27-gauge needle facilitated placing the top-view camera exactly above the needle to visualize the drop during its impact and spreading. The average drop diameters were about 1.97 mm for epoxy resin, 1.99 mm for epoxy hardener, 1.95 mm for epoxy resin and hardener, 1.75 mm for silicone oil, and 1.90 mm for turpentine oil mixed the oil-soluble aniline dyes, when the 27-gauge needle was used. The drops detached and fell onto the balsa or polypropylene substrates due to gravity, and thus, the impact velocity was controlled by the height of the needle tip. Accordingly, the average impact velocities recorded in the side view by the high-speed camera (Phantom V210) were 1.53, 1.47, 1.51, 1.49, and 1.51 m/s for epoxy resin, epoxy hardener, epoxy resin and hardener, silicone oil, and turpentine oil, respectively. The aerodynamic drag made these values slightly lower than the estimate of $\sqrt{2gh} = 1.57\,\mathrm{m/s}$, where g is the gravity acceleration. In all cases studied in this work, the drop impact was normal to the balsa and polypropylene substrates.

In order to visualize the side and top views of drop impact, two high-speed cameras (Phantom V210 and Phantom Miro 4) were employed. For the side viewing, a back-lighting (LED lamp) illuminated the drop, and for the top viewing front lighting was used. In recording the side views, the camera was aligned at the same vertical level as that of the corresponding substrates. Then, the images from the high-speed recordings were analyzed in Adobe Photoshop, MATLAB, and ImageJ. The impact velocity was determined by the drop motion observed in the side view. All the experiments were performed at room temperature.

The physical properties of the working fluids used in the experiments are listed in Table I. For convenience, note that conversion of the SI unit for the electric conductivity (S/cm) into the corresponding Gaussian (CGS) unit is as follows: $1\ \mathrm{S/cm} = 9 \times 10^{11}\ \mathrm{s}^{-1}$. The charge relaxation time of the fluid expressed in the CGS units is given by $\tau = \varepsilon/4\pi\sigma$, where ε is the dielectric permittivity and σ is the electrical conductivity. For silicone and turpentine oils, $\tau = 20$ s and $\tau = 24.4$ s, respectively.

For each fluid used in the experiments (epoxy resin, epoxy hardener, epoxy resin and hardener, silicone, and turpentine oils), six and eight consecutive drop impact trials were conducted in each case without and with the applied electric field, respectively. It should be emphasized that the data reported in the present work are fully representative of all the experimental results, because the dynamics of impact and spreading were similar in the other trials corresponding in each case and for both dielectric substrates employed here.

The static contact angle measurements for all these fluids on balsa wood and polypropylene substrates were conducted with drops softly placed on it without and with the electric field applied. Note that each contact angle measurement was carried out using a new balsa substrate. The measurements were conducted using the snapshots from the side views and ImageJ tool. The reported contact angle for each fluid is the average value measured on both sides of the drop, with an error within $\pm 2°$. In each case, three different measurements were conducted for each fluid used in the present experiments (epoxy resin

TABLE I. Properties of fluids used in the experiments. The data corresponding to epoxy resin and hardener are found in the instructions sheet from the manufacturer, and for silicone and turpentine oils is available in Granda *et al.* (2022a) and Granda *et al.* (2021b), respectively.

Fluid/property	Density ρ (kg/m^3)	Kinematic viscosity ν (cm^2/s)	Surface tension γ (mN/m)	Relative dielectric constant (dielectric permittivity) ε	Electrical conductivity of liquid σ (S/cm)
Epoxy resin	1150	23.913	Unavailable	Unavailable	Unavailable
Epoxy hardener	950	5.526	Unavailable	Unavailable	Unavailable
Silicone oil	970	5.092	21.1	2.76	10^{-14}
Turpentine oil	862	0.0173	27	2.25	10^{-14}

TABLE II. Static contact angles for epoxy resin, epoxy hardener, epoxy resin and hardener, and silicone oil on balsa wood and polypropylene substrates without and with the electric field.

Fluid and substrate	Static contact angle at 0 kV (°)	Static contact angle at 10 kV (°)
Epoxy resin on polypropylene	65	14
Epoxy resin on balsa wood	43	37
Epoxy hardener on polypropylene	48	22
Epoxy resin and hardener on polypropylene	51	32
Silicone oil on balsa wood	23	22

and hardener, epoxy resin and hardener, silicone oil, and turpentine oil with oil-soluble aniline dyes).

Note that data for the contact angle of turpentine oil with aniline dyes on balsa wood are not listed in Table II due to an immediate imbibition of drops into the porous surface following soft deposition onto it.

The present experiments with the electric field were conducted up to the 10 kV voltage based on the experience in the prior works of the present group. The previous multiple tests and experimental data on impact of aqueous and hydrocarbon liquids without and with particles revealed no electric discharges before the corona discharge (a spark in air) at the voltage of ∼10.5 kV for the 1.5 cm separation between the copper electrodes. The voltage range of 0 kV up to 10 kV was used as a safety measure when performing the experiments, which helps to avoid electrical sparks.

III. EXPERIMENTAL RESULTS AND DISCUSSION

A. Drops of epoxy resin and epoxy hardener on balsa wood and polypropylene substrates

Single drops of pure epoxy resin dripped onto the balsa wood and polypropylene substrates from a fixed height of 12.5 cm. The top view recorded by a high-speed camera captured the collision and evolution of drops at a rate of 500 fps for both types of substrates. It should be emphasized that the choice of the camera rate here and hereinafter (where 1000 fps would be used) was dictated by the necessity to record details of drop evolution in time, which were affected by particular fluid and substrate properties. Figure 2 depicts the recorded spreading achieved by the drop after it impacted onto the dielectric surfaces when no electric field was applied [Figs. 2(a) and 2(c), Multimedia view] for polypropylene and balsa wood surfaces, respectively, whereas the electrically driven spreading achieved by the drop with DC voltage applied is illustrated in Figs. 2(b) and 2(d) (Multimedia view). Splashing criteria corresponding to drop impact involve the dimensionless K number $K = We\,Oh^{-2/5}$, where We is the Weber number defined as $We = \rho DV^2/\gamma$ and Oh is the Ohnesorge number $Oh = \mu/\sqrt{\rho D\gamma}$, with ρ being the fluid density, D the initial diameter of the drop, V the velocity of the drop before impact, and γ and μ the surface tension and dynamic viscosity of the liquid, respectively. Also, in the following experimental datasets, the dimensionless electric capillary number defined as $Ca_E = \varepsilon E^2 r/\gamma$ will be used to characterize the effect of the electric field, where ε is the dielectric permittivity of the exterior fluid (air, with $\varepsilon \approx 1$), E is the applied electric field strength between the electrodes, and $r = D/2$ is the initial radius of the drop. In this particular case of pure epoxy resin, the average diameter of each drop before the impact was ∼1.97 mm, and the impact velocity was ∼1.53 m/s in all the trials.

Figures 2(a) and 2(b) (rows 1–4) reveal a significantly different drop spreading behavior of epoxy resin drops on polypropylene substrate when an in-plane electric field is applied compared to the case without the electric field. Note that epoxy resin does not wet polypropylene. After drop impact, at t = 1 s, the epoxy resin drop experiences the electrically driven stretching toward both electrodes. This stretching effect persists as time progresses increasing the wetted area. Such a stretching reveals some minor irregularities in its shape related to the applied electric force and the roughness of polypropylene [cf. the snapshots at t = 14 s and t = 16 s in Fig. 2(b)]. On the other hand, Figs. 2(c) and 2(d) (Multimedia view) reveal a significant effect of wettability of balsa wood by epoxy resin in the dynamics of drop evolution. The epoxy resin wets balsa wood, and thus, the wettability-driven spreading is felt even without the electric field applied [cf. Fig. 2(c), Multimedia view]; however, the electrically driven spreading adds significantly to the wettability-driven spreading [cf. Fig. 2(d), Multimedia view]. It should be emphasized that the electrically driven spreading of epoxy resin on balsa wood is more significant than that of the aqueous drops with aniline dye explored in the previous work of this group (Granda *et al.*, 2022b). This is because the wettability-driven imbibition of the epoxy-resin into balsa wood is much less than of the aqueous drops with aniline dye into balsa wood. Accordingly, in the present case of the epoxy resin, a significant part of the fluid stays over the surface and sustains strong enough Maxwell stresses stretching the drop. Note that stretching continued for several more seconds after t = 16 s in Fig. 2(d) (Multimedia view). It is worth noting that the snapshots shown in Fig. 2 (rows c and d) revealed no finger formation due to prompt splashing or the electric field applied. The roughness of the balsa wood substrates did not generate prompt splashing at the advancing contact line at 0 kV. When a 10 kV voltage was applied to the dielectric balsa surface, all trials revealed a slight increase in the wetted area compared to the case without voltage applied. Moreover, viscosity and surface tension of epoxy resin could be responsible for the absence of fingers with the electric field applied [epoxy resin is about 2300 times more viscous than turpentine oil (which reveals fingering with the application of the electric field)]. Also, a low ion and counterion concentration in epoxy resin could be a reason that the electric Maxwell stresses are not severe enough to cause an instability (protrusions) at the drop rim that could trigger finger growth.

Additional experiments with epoxy hardener and epoxy resin and hardener impacts onto polypropylene substrate without and with the electric field applied were performed. It is worth mentioning that a new polypropylene substrate was used for each trial conducted at 0 and 10 kV. The average diameter of each drop before the impact was ∼1.99 and ∼1.95 mm, and the impact velocities were ∼1.47 and ∼1.51 m/s in all the trials for epoxy hardener and epoxy resin and hardener, respectively. The results for drops of epoxy hardener are presented in Fig. 3, whereas those for epoxy resin and hardener are shown in Fig. 4. In the particular case of the snapshots in Fig. 3 (row b), the drop impacted slightly off the center of the polypropylene substrate area [a little bit leftward and against the direction of the electric field (from the left to the right)] due to the uncontrollable drop oscillations

FIG. 2. Snapshots of drops of epoxy resin impact onto polypropylene and balsa wood substrates. Row (a): 0 kV on polypropylene substrate. Row (b): 10 kV (the electric field strength of 6.6×10^5 V/m) on polypropylene substrate. Row (c): 0 kV on balsa wood substrate. Row (d): 10 kV (the electric field strength of 6.6×10^5 V/m) on balsa wood substrate. The left-hand side electrode is the anode and the right-hand side one is grounded (the cathode). The time moments are listed in each image. The inter-electrode distance is 1.5 cm. Scale bar is 2 mm. Multimedia available online.

in flight before impact. However, a more pronounced stretching/deformation still happens toward the right, in the direction of the field lines, probably due to an initial shape acquired by the drop in this case. The additional trials conducted under the same experimental conditions also revealed a similar pattern. It should be emphasized that the snapshots in Fig. 3 are fully representative of all the additional trials conducted with epoxy hardener.

The comparison of Fig. 3 to Figs. 2(a) and 2(b) reveals a similar trend in spreading of drops of epoxy hardener and of epoxy resin, respectively, when no electric field is applied to the dielectric surface. Drop evolution as time progresses reveals a relatively larger area covered by the spreading epoxy hardener drop at $t = 16$ s [Fig. 3(a)] compared to the epoxy resin drop in Fig. 2(a) at the same time moment. On the other hand, the presence of the electric field resulted in strong stretching of the epoxy hardener drop toward both electrodes. The strong electric field strength of 6.6×10^5 V/m facilitated stretching of the hardener drop (Fig. 3) compared to that of the epoxy drop [Fig. 2(b)] because of a lower viscosity of epoxy hardener compared to that of epoxy resin. The slightly diminished drop stretching in Fig. 2(b) in comparison with Fig. 3(b) is caused by a higher viscous dissipation in the former case of epoxy resin. It should be emphasized that a relatively symmetric drop stretching is visible for the epoxy

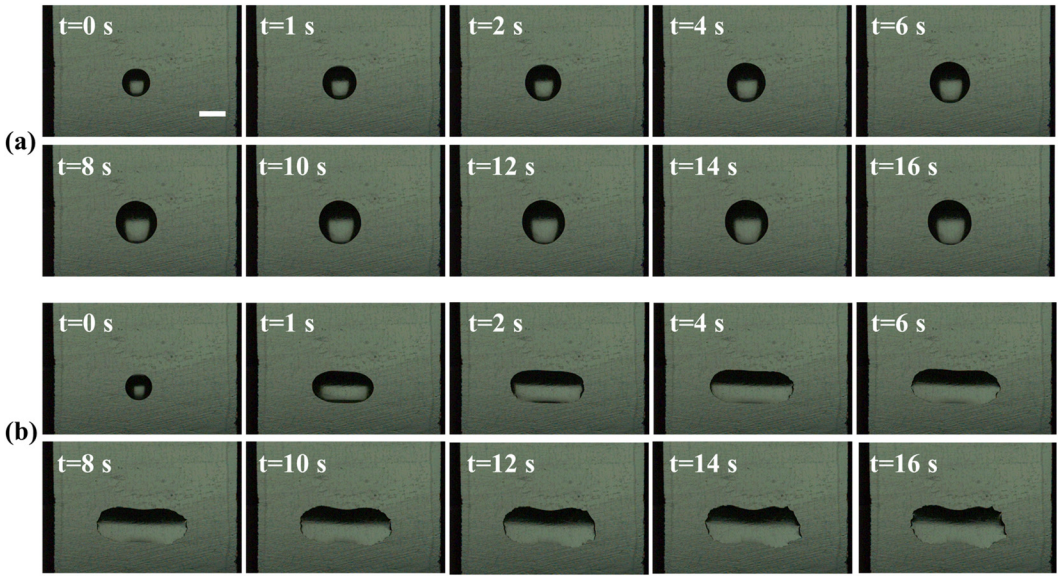

FIG. 3. Snapshots of drops of epoxy hardener impacting onto: (a) and (b) polypropylene substrate, and (c) and (d) balsa wood substrate. Rows (a) and (c) without electric field applied, and (b) and (d) at the applied voltage of 10 kV corresponding to the electric field strength 6.6×10^5 V/m. The left-hand side electrode is the anode and the right-hand side one is grounded (the cathode). The time moments are listed in each image. The inter-electrode distance is 1.5 cm. Scale bar is 2 mm.

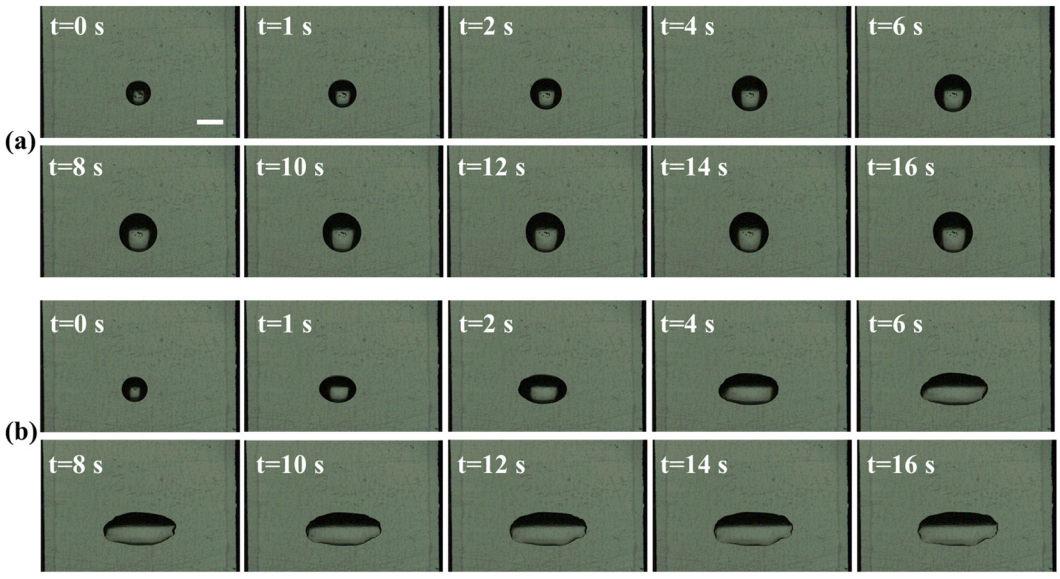

FIG. 4. Snapshots of drops of epoxy resin and hardener impacting onto: (a) and (b) polypropylene substrate, and (c) and (d) balsa wood substrate. Rows (a) and (c) without electric field applied, and (b) and (d) at the applied voltage of 10 kV corresponding to the electric field strength 6.6×10^5 V/m. The left-hand side electrode is the anode and the right-hand side one is grounded (the cathode). The time moments are listed in each image. The inter-electrode distance is 1.5 cm. Scale bar is 2 mm.

hardener drop during the first seconds after impact onto polypropylene surface (Fig. 3). Then, at $\sim t = 12$ s, the rim of the spreading drop develops some tiny perturbations in the form of dendrites especially visible at the left- and right-hand side edges at $t = 16$ s.

Experiments with drops of a mixture of epoxy resin and hardener were also carried out on polypropylene substrate. Figure 4 presents the recorded shape evolution and stretching in drops after they impacted onto the dielectric surface without and with an applied voltage of 10 kV corresponding to the electric field strength of 6.6×10^5 V/m. Note that the voltage was applied before the drop impact. It should be emphasized that the snapshots in Fig. 4, as before, are fully representative of all the additional trials conducted, because similar

impact dynamics and spreading were observed for both cases at 0 and 10 kV.

Similarly to Figs. 2(a) and 3(a), in Fig. 4(a), in the case without voltage applied, i.e., at 0 kV, the epoxy resin and hardener drop spreads relatively slowly over the surface only due to the impact inertia and wettability, affected by surface tension and viscous dissipation in the 0–16 s time range, and at t = 16 s, its evolution comes to rest. Note also that in the case with the applied voltage of 10 kV [Fig. 4(b)], the drop spreading and evolution do not significantly differ from the cases of epoxy resin and epoxy hardener in the time frame of 0–6 s (row 3 in Figs. 2 and 3, respectively). However, the snapshots from the 8–16 s interval reveal a slight change in the spreading rate and the shape of epoxy resin and hardener drops compared to those of unmixed epoxy resin and hardener alone. In particular, Fig. 4(b) reveals that the mixed epoxy resin and hardener drop stretched by the electric forces (the Maxwell stresses) acquires an almost perfectly elliptic shape, in distinction from Figs. 2(b) and 3(b) corresponding to the unmixed epoxy resin and epoxy hardener drops, respectively, which in turn, reveal small distortions along the lateral rims that grow as time progresses up to the t = 16 s moment. The mixture of both fluids (epoxy resin and epoxy hardener), which differ in their viscosities, explains the change in the evolution dynamics and drop shape on the same type of dielectric substrate and at the same electric field strength applied. It should be emphasized that solidification in the mixture of epoxy resin and hardener would begin to take place on the scale of 40 min (according to the manufacturer) and, thus, is immaterial for all the experiments in the present work conducted at a much shorter timescale.

Note that at the frame rate used in the experiments depicted in Fig. 4 (500 fps), drop evolution with the electric field applied was recorded for another 5 s (21 s in total) to observe any additional effect of the electric force on the epoxy resin and hardener drops. Since no visible changes in the drop shape had been seen, the experimental results are reported here only until t = 16 s after drop impact for both cases without and with the electric field applied, similarly to Figs. 2 and 3 for unmixed epoxy resin and epoxy hardener, respectively.

B. Drops of silicone oil on balsa wood substrate

Single drops of silicone oil dripped onto balsa wood substrate from a fixed height of 12.5 cm. The top views recorded by a high-speed camera (Phantom Miro 4) captured the drop evolution and spreading at the rate of 1000 fps for all trials conducted without and with the electric field applied. Figure 5 illustrates the evolution of drops of silicone oil on the dielectric porous surface without the electric field applied and with the applied voltages of 7 and 10 kV (rows 1–3, respectively). It should be emphasized that in our previous work (Granda *et al.*, 2022a), it was found that ion concentration in silicone oils is insufficient to sustain any significant Maxwell stresses, which means that silicone oils by themselves are practically unaffected by the electric field. The average diameter of each drop before the impact was ∼1.75 mm, and the impact velocity was ∼1.49 m/s, in all trials conducted. It should me mentioned that in each case, a new balsa wood substrate was used, so different grooves patterns are visible in the images below.

In Fig. 5, the snapshots at t = 0 s corresponds to the moment of the drop impact onto a balsa wood surface. The snapshots reveal the wettability-driven spreading of drops of silicone oil in all the cases studied without and with the electric field applied (rows 1–3). Note that without the electric field applied, i.e., at 0 kV, the silicone oil drop relatively slowly evolves only due to the inertia, wettability, being affected by surface tension and viscous dissipation in the 1–7 s time

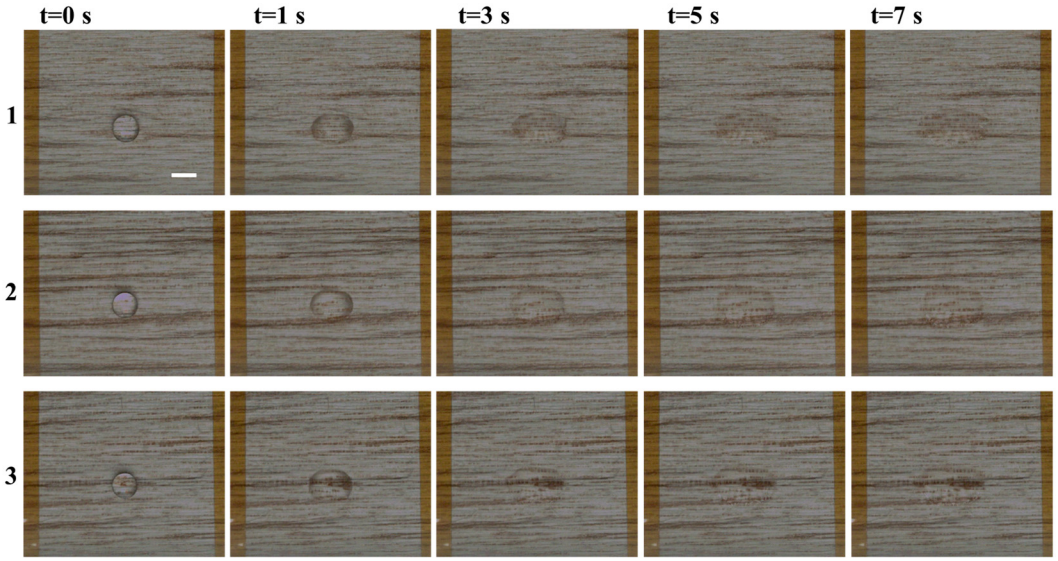

FIG. 5. Snapshots of drops of silicone oil impacting on a balsa wood substrate without the electric field applied (row 1) and at the applied voltages of 7 and 10 kV (rows 2 and 3) corresponding to the electric field strengths of 4.6×10^5 V/m and 6.6×10^5 V/m, respectively. The left-hand side electrode is the anode, and the right-hand side one is grounded (the cathode). The time moments are listed on top of the columns. The Weber number We = 178.6, the Ohnesorge number Oh = 2.61, and the composite parameter K = 121.7. The electric capillary numbers are $Ca_E = 1.004$ and $Ca_E = 2.047$ for 7 and 10 kV, respectively. (Note that for fluids employed in the experiments corresponding to Figs. 2–4 dimensionless groups, unfortunately, cannot be provided because some material parameters are unknown for those commercial products). The inter-electrode distance is 1.5 cm. Scale bar is 2 mm.

range. Note that in the process of imbibition through porous balsa, 33%–35% of the silicone oil drop remained over the surface and about 65%–67% left was imbibed when the recording was finished at ∼7 s. Essentially imbibition of silicone oil into balsa wood was more intense than the epoxy resin imbibition into balsa. The imbibition percentage values mentioned above were evaluated as follows. First, the initial drop radius was measured in the experiments, and the corresponding initial drop volume was calculated. Then, using the measured wetted areas at 0 kV listed in Table III and the average equivalent drop height over the surface the volume of liquid remaining over the surface was calculated. Finally, with the initial drop volume and the volume of liquid remaining over the surface, one can calculate the volume of liquid imbibed into the balsa surface. The average of those results corresponding to all the six trials conducted yields the percentage values in the 33%–35% range of liquid remaining over the surface and the imbibition of 65%–67%.

The imbibition of silicone oil into balsa wood is corroborated by the following data from the literature. Cai *et al.* (2023) used balsa wood with similar properties like the present balsa specimens in terms of the density, pore sizes, and porosity and reported silicone oil absorption into balsa. Additionally, Fu *et al.* (2018) also used balsa wood with similar properties in terms of density and porosity, like the present one and reported absorption of silicone oil (without specifying its properties). In Perré *et al.* (2022), poplar and spruce wood samples were used with water and silicone oil and imbibition was reported. The silicone oil used by Perré *et al.* (2022) possessed almost the same density value as the one used in the present experiments (∼1000 kg/m^3), the same surface tension value of 0.021 N/m, but a lower viscosity of 0.02 Pa s vs the one in the present silicone oil of 0.49 Pa s). Note that poplar and spruce wood are quite similar in their physical properties: ∼70% to 76% porosity (Jang *et al.*, 2019; Plötze and Niemz, 2011; Šoškić *et al.*, 2007; and Zhou *et al.*, 2018), ∼350 to 520 kg/m^3 density (Jang *et al.*, 2019; Plötze and Niemz, 2011; Šoškić *et al.*, 2007; Wood–Densities of Various Species, 2001; and Zhou *et al.*, 2018), and ∼0.5–58 μm in pore sizes (Jang *et al.*, 2019; Plötze and Niemz, 2011; and Zhou *et al.*, 2018). In comparison, for balsa wood (including the type of balsa used in the present experiments), the properties are mentioned in the literature: ∼87.3% to 93.2% porosity (Cai *et al.*, 2023; Fu *et al.*, 2018), ∼108 to 191 kg/m^3 density (Cai *et al.*, 2023; Fu *et al.*, 2018; and Wood–Densities of Various Species, 2001), and ∼8 to 52 μm in pore sizes (Cai *et al.*, 2023). Accordingly, there is clear evidence of imbibition of silicone oil in balsa wood and other types of wood similar to balsa (poplar and spruce).

It should be emphasized that in the cases with the voltages of 7 and 10 kV applied (rows 2 and 3 in Fig. 5), the drop evolution does not differ from that without the electric field (0 kV, row 1). This means that drops of silicone oil do not react to the electric field, in particular, and are not stretched by it, in distinction from the other liquids studied and described above (epoxy resin and hardener). Accordingly, one can conclude once again that concentration of preexisting ions in silicone oil is so low (if there are any, at all) that its drops do not experience any measurable stretching driven by the Maxwell stresses in distinction from the other liquids discussed above. Additionally, note that a significant part of silicone oil still remained over the surface of the balsa substrates in the cases with the electric field applied at 7 and 10 kV (rows 2 and 3 in Fig. 5), which resembles the case without voltage at 0 kV.

Furthermore, at the frame rate (1000 fps) used in the experimental results depicted in Fig. 5, drop spreading was recorded after impact for about 7 s. For the cases with the electric field, the applied voltage had been turned on before drop impact onto the porous balsa surface.

Note that silicone oil is a synthetic compound with chains of oxygen atoms bonded to silicon atoms. Its different chemical structure and the manufacturing processes determine the lower concentration of preexisting ions in silicone oil.

C. Drops of turpentine oil with aniline dyes on balsa wood substrate

Drop impact experiments were conducted using turpentine oil (an organic solvent extracted predominantly from pine trees) on balsa wood substrate. The recorded impact dynamics and spreading of drops of turpentine oil mixed with oil-soluble golden yellow oak aniline dye at concentration of 7 wt. %, at different applied voltages is illustrated in Fig. 6. The top view evolution was recorded at an acquisition rate of 1000 fps. The snapshots in Fig. 6 cover the millisecond to second range to elucidate the short and long terms drop evolution before it reaches the copper electrodes. The average diameter of each drop before the impact was ∼1.90 mm, and the impact velocity was ∼1.51 m/s in all the trials without and with the electric field.

Row 1 in Fig. 6 corresponding to drops of turpentine oil mixed with golden yellow oak aniline dye reveals the formation of fingerlike structures along the rim of the drop for the case without the electric field applied. After the drop impact, at 4 and 14 ms, the drop also

TABLE III. Wetted areas of epoxy resin, epoxy hardener, epoxy resin and hardener, silicone oil, and turpentine oil with aniline dyes recorded after drop impact onto balsa wood and polypropylene substrates without and with the applied voltage of 10 kV at t = 16 s (except the results marked by * and ** corresponding to t = 7 s and t = 0.5 s, respectively).

Fluid and substrate	Area at 0 kV (mm^2)	Area at 10 kV (mm^2)	Percentage increase (%)
Epoxy resin on polypropylene	7.71 ± 0.49	15.04 ± 0.83	95.1 ± 1.7
Epoxy resin on balsa wood	10.67 ± 0.44	16.06 ± 0.24	50.5 ± 3.8
Epoxy hardener on polypropylene	10.11 ± 1.08	20.76 ± 0.71	105.3 ± 16.7
Epoxy resin and hardener on polypropylene	8.20 ± 0.66	14.29 ± 0.63	74.3 ± 6.9
Silicone oil on balsa wood	16.31 ± 0.27*	16.17 ± 0.91*	−0.85 ± 5.7*
Turpentine oil with golden yellow oak dye (7 wt.%) on balsa wood	24.34 ± 0.71**	26.40 ± 0.72**	8.5 ± 0.4**
Turpentine oil with black dye (10 wt.%) on balsa wood	26.32 ± 1.33**	27.34 ± 1.16**	3.9 ± 0.9**

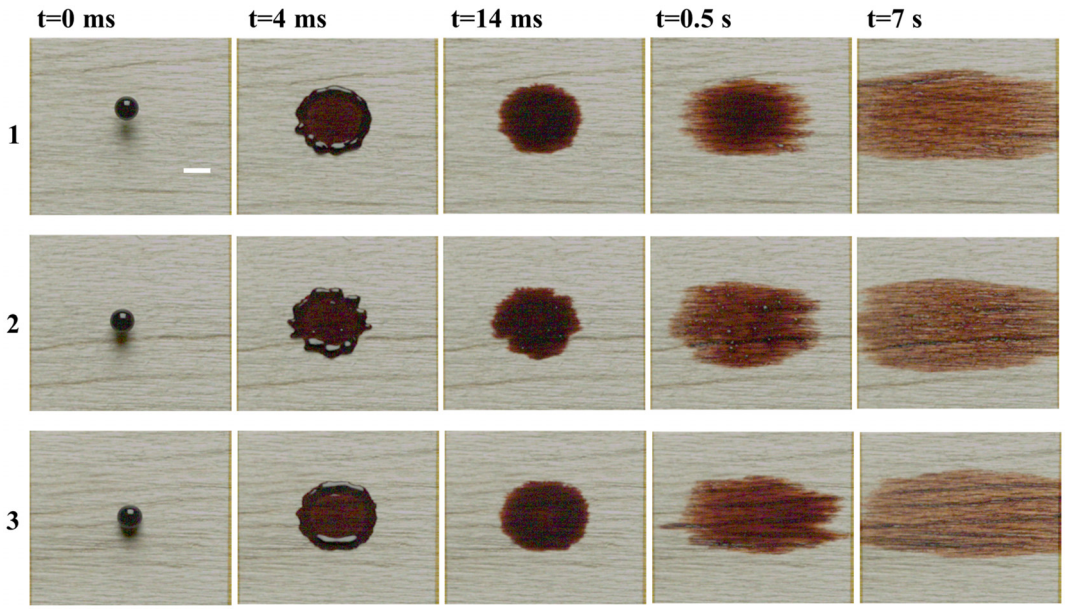

FIG. 6. Snapshots of drops of turpentine oil with golden yellow oak dye (7 wt. % concentration) impacting onto a balsa wood substrate without the electric field applied (row 1) and at the applied voltages of 7 and 10 kV (rows 2 and 3) corresponding to the electric field strengths of 4.6×10^5 and 6.6×10^5 V/m, respectively. The left-hand side electrode is the anode, and the right-hand side one is grounded (the cathode). The time moments are listed on top of the columns. The Weber number We = 138.3, the Ohnesorge number Oh = 0.007, and the composite parameter K = 1001.4. The electric capillary numbers are $Ca_E = 0.851$ and $Ca_E = 1.737$ for 7 and 10 kV, respectively. The inter-electrode distance is 1.5 cm. Scale bar is 2 mm.

reveals wettability-imbibition-driven spreading during the advancing motion. Furthermore, the application of the electric field of the strengths of 4.6×10^5 and 6.6×10^5 V/m, corresponding to the applied voltages of 7 and 10 kV (rows 2 and 3, respectively), reveals a minimum effect compared to the case at 0 kV (row 1). On the contrary, drop impact on solid polypropylene substrate reveals a significant stretching of the spreading drops accompanied by small dendrite-like structures formed along the rim, as demonstrated in Granda *et al.* (2021b). It should be emphasized that the images at t = 0 ms correspond to the time moment of the initial contact of the drops with balsa wood surface. Also, the snapshots at t = 0.5 s and t = 7 s reveal a slight increase in the painted area by the electric force in the long-term high-speed recordings. This painted area ultimately forms a strip of paint connecting both electrodes similarly to aqueous suspensions with water-soluble aniline dyes explored in the previous work of the present group (Granda *et al.*, 2022b).

Experiments with additional aniline dyes of different pigment colors were also conducted using balsa wood substrate. Figure 7 presents the recorded overall evolution of drops of turpentine oil mixed with oil-soluble black aniline dye (10 wt. % concentration), after they impacted onto the balsa wood surface subjected to different applied voltages. Again, the snapshots in Fig. 7 cover the millisecond to second range to elucidate the spreading dynamics and dye-covered area of the drops before they reached the electrodes. The average diameter of each drop before the impact was ~1.90 mm, and the impact velocity was 1.51 m/s in all the trials conducted. It should be emphasized that in each case, a new balsa wood substrate was used, so different groove patterns are visible in the images below.

Figure 7 reveals a similar trend (up to the 14 ms time moment) in the drop spreading dynamics with the wettability-imbibition-driven phenomenon as shown in Fig. 6 for the case of turpentine oil with golden yellow oak aniline dye. Moreover, in Fig. 7 at t = 0.5 s and t = 7 for the cases without and with the electric field (rows 1–3), the snapshots demonstrate a slightly smaller and less prominent painted areas with the black aniline dye. This is due to different pigment colors and dye concentrations used in these experiments. In particular, the golden yellow oak aniline dye reveals a more prominent coloration at the chosen concentration of 7 wt. % than the black dye at 10 wt. %. Furthermore, the drops of turpentine oil with black aniline dye reveal some fingerlike structures along the lateral rims of the drops which become slightly more pronounced at the applied voltages of 7 and 10 kV (at t = 4 ms after drop impact in Fig. 7) in contrast to those after impact onto polypropylene surface in Granda *et al.* (2021b). In the latter work, dendrite-like fingers grew from the impacting drops and rapidly reached the cooper electrodes. Additionally, the snapshots in Figs. 6 and 7 reveal that the effect of wettability-driven imbibition and spreading in the long-term is more significant than the effect of the electric field, which, in turn, results in a significant decrease in the part of the drop remaining above the porous surface and capable to sustain the electric Maxwell stresses. Hence, drops of turpentine oil with dyes rapidly penetrate into balsa pores and impregnate such a substrate.

Drop evolution under the action of the electric Maxwell stresses is associated with the ion motion to the free surface. The charge layer at the free surface is capable of interaction with the electric field in the drop exterior, thus creating the Coulomb forces expressed by the Maxwell stresses. The characteristic time of charge motion is the charge

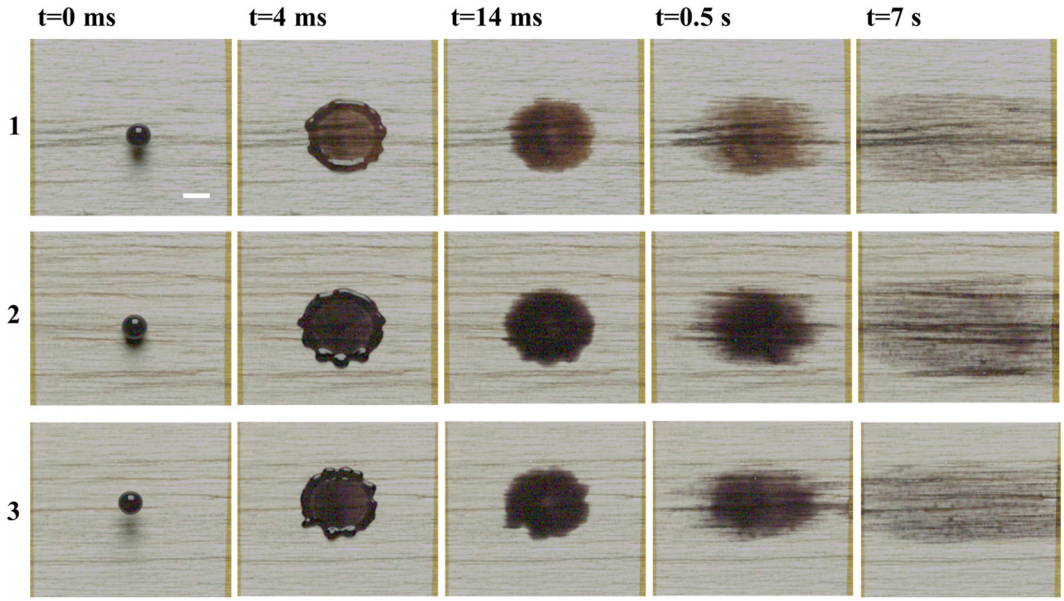

FIG. 7. Snapshots of drops of turpentine oil with black aniline dye (10 wt. % concentration) impacting onto a balsa wood substrate without the electric field applied (row 1) and at the applied voltages of 7 and 10 kV (rows 2 and 3) corresponding to the electric field strengths of 4.6×10^5 and 6.6×10^5 V/m, respectively. The left-hand side electrode is the anode, and the right-hand side one is grounded (the cathode). The time moments are listed on top of the columns. The Weber number We = 138.3, the Ohnesorge number Oh = 0.007, and the composite parameter K = 1001.4. The electric capillary numbers are $Ca_E = 0.851$ and $Ca_E = 1.737$ for 7 and 10 kV, respectively. The inter-electrode distance is 1.5 cm. Scale bar is 2 mm.

relaxation time $\tau_C = \varepsilon/(4\pi\sigma_e)$, where ε is the dielectric permittivity of liquid in the drop, and σ_e is the electrical conductivity (here, the CGS units are used); Yarin *et al.* (2019). The electrical conductivity is expressed as $\sigma_e = 2c_\infty De^2/k_BT$, where c_∞ is the cation or anion concentration in the electroneutral liquid far from the free surface, D is the ion diffusion coefficient, e is the proton charge (monovalent ions are implied), k_B is Boltzmann's constant, and T is the temperature. The characteristic restraining hydrodynamic time $\tau_H \sim \mu a/\sigma$, where μ and σ are the viscosity and surface tension of the liquid, respectively, and a is the volume-equivalent drop radius. Drop evolution under the action of the applied field would be impossible, if $\tau_C \gg \tau_H$ (Yarin *et al.*, 2019), which yields the following criterion for the ion concentration

$$c_\infty \ll \frac{\varepsilon k_B T \sigma}{8\pi De^2 \mu a}. \quad (1)$$

The latter means that if the ion concentration in liquid is low, then the drop stretching by the Maxwell stresses would be impossible.

On a fully wettable intact (non-porous) surface, the characteristic hydrodynamic time estimate by using the Hoffman–Voinov–Tanner law is $\tau_H \sim \mu a/\sigma$, where surface tension is the measure of the wettability-driving force, the surface tension of the solid-gas substrate (Yarin *et al.*, 2019). Accordingly, the same estimate (1) holds for the low ionic concentrations, at which wettability, rather than the Maxwell stresses, would dominate. Also, because imbibition is, essentially, driven by wettability of pore surfaces, the estimate of Eq. (1) holds for drops on porous surfaces as well.

An example of liquids with extremely low ion concentrations is the silicone oils; in such cases, only dielectrophoretic drop stretching is possible (Granda *et al.*, 2022a). The Coulomb force (expressed through the Maxwell stresses) acting on a drop is estimated as $F_M \sim \sigma_s a^2 E_\infty$, where σ_s is the surface charge density, and E_∞ is the characteristic electric field strength. On the other hand, assuming that a drop on the surface is surrounded by air with dielectric permittivity of 1, the force of the dielectrophoretic origin acting on a drop is estimated as $(\varepsilon-1)a^3/[2(\varepsilon+2)]\nabla E_\infty^2 \sim (\varepsilon-1)a^2/[2(\varepsilon+2)]E_\infty^2$ (Pohl, 1978; Granda *et al.*, 2022a). Accordingly, the ratio of the dielectrophoretic to Coulomb stretching forces is of the order of

$$R \sim \frac{(\varepsilon-1)E_\infty}{2(\varepsilon+2)\sigma_s}. \quad (2)$$

Moreover, adding particles to aqueous and hydrocarbon solvents modifies to some extent the electrical conductivity of fluid and adds dielectrophoretic stretching (Granda *et al.*, 2021a, 2022a).

D. Footprint area and the electric field effect

An important feature associated with the observed drop evolution is the footprint area as a function of time. The footprint evolution (i.e., the visible wetted area) of the drops on the dielectric substrates was analyzed using the experimental observations for drops of epoxy resin, epoxy hardener, epoxy resin and hardener, silicone oil, and turpentine oil with aniline dyes on balsa wood and polypropylene substrates. The evolution of the footprint areas obtained from the top views for each set of experiments (Figs. 2–7) without and with application of the electric field is illustrated in Figs. 8–10. Note that the centers of the drops

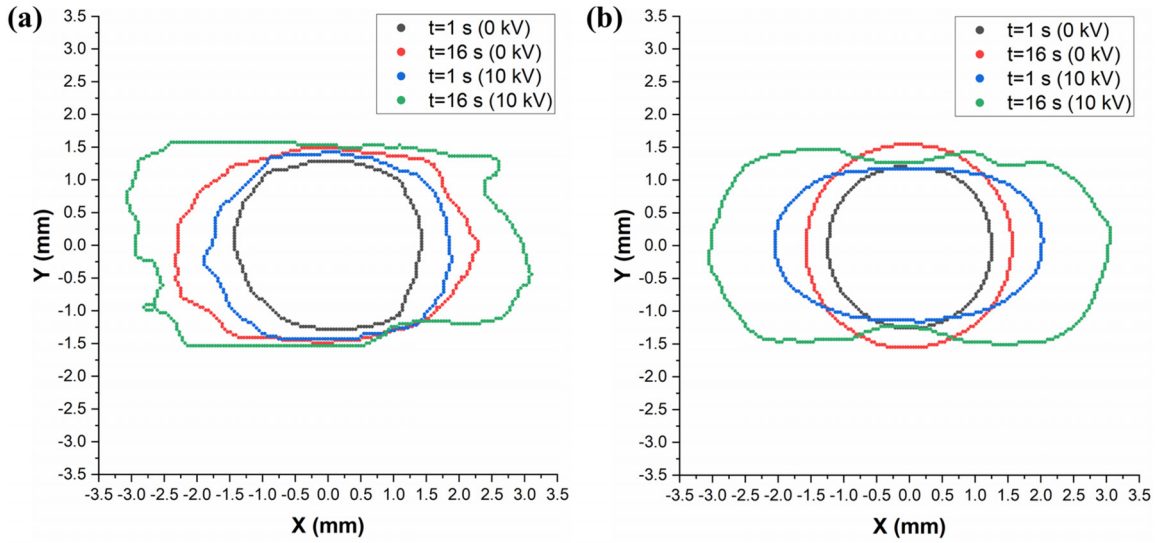

FIG. 8. Footprint area contours of drops of epoxy resin drops on (a) balsa wood and (b) polypropylene substrates without and with the electric field observed after impact in the top view. The left-hand side electrode is the anode, and the right-hand side one is grounded (the cathode). The Cartesian coordinates on the substrates are denoted as x (in the field direction) and y.

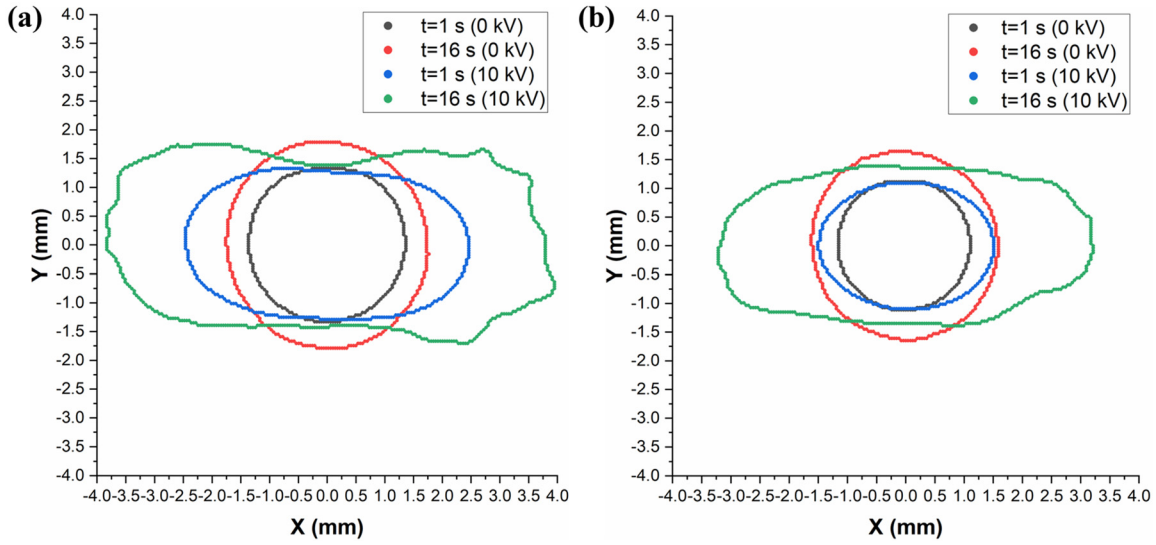

FIG. 9. Footprint area contours of drops of (a) epoxy hardener and (b) epoxy resin and hardener on polypropylene substrate without and with the electric field observed in the top view. The left-hand side electrode is the anode and the right-hand side one is grounded (the cathode). The Cartesian coordinates on the substrates are denoted as x (in the field direction) and y.

analyzed were located very closely in all cases, with an offset of only a few pixels in the images due to the uncontrollable drop oscillations in flight before impact. The drop contour traces observed in the experiments on the balsa wood and polypropylene substrates with drops of pure epoxy resin (Fig. 2) are depicted in Fig. 8. The superposition of the wetted area contours measured at the time moments t = 1 s and t = 16 s without the electric field applied and at the applied voltage of 10 kV (the electric field strength of 6.6×10^5 V/m) reveals the effect of the electric forces (the Maxwell stresses) on the drop spreading and evolution on both dielectric surfaces explored.

The applied electric field enhances spreading on both dielectric surfaces as expressed by an increase in the wetted area, which appears to be stretched along the x-axis in Fig. 8(b) for polypropylene substrate. An increase in the footprint area on the balsa wood substrate reveals the flow behavior of epoxy resin on the porous surface when the

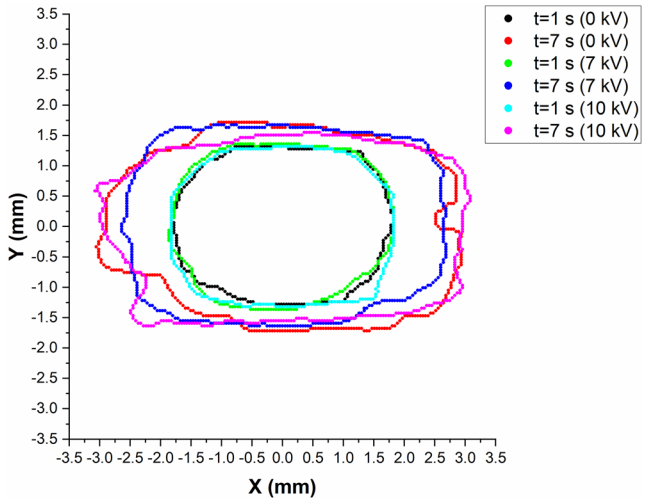

FIG. 10. Footprint area contours of drops of silicone oil on a balsa wood substrate without and with the electric field after impact as experimentally observed in the top view. The left-hand side electrode is the anode, and the right-hand side one is grounded (the cathode). The Cartesian coordinates on the substrate are denoted as x (in the field direction) and y.

voltage is applied. Here, wettability-driven spreading with partial imbibition is enhanced by the electric field compared to the case at 0 kV as seen in Fig. 8(a). The footprint envelope evolution in the case of 10 kV on polypropylene reveals a slightly larger wetted area at $t = 16$ s in comparison with that on the balsa wood at the same time moments. The comparison of the footprint areas without and with voltage is possible because all the contours are superimposed at the center of each substrate to elucidate the effect of the electric field on surfaces with different roughness and wettability. Furthermore, Fig. 8(b) reveals that the drop spreading is affected by the electric field triggering some small distortions on the drop rim in the case of polypropylene substrate. Also, drop stretching along the x axis toward both electrodes with the electric field applied indicates the action of the Maxwell stresses and thus the preexistence of anions and cations in epoxy resin.

The contour traces of the spreading drops corresponding to the observations in Figs. 3 and 4 (pure epoxy hardener and the mixture of epoxy resin and hardener, respectively) on polypropylene surface are depicted in Fig. 9. The superposition of the drop wetted areas without the electric field (at 0 kV) and with application of a 10 kV DC voltage reveals the effect of the stretching electric forces acting on the drops, with the maximum drop stretching corresponding to the case of 10 kV.

Each panel in Fig. 9 allows for a direct comparison between the drop shape before and after voltage has been applied on polypropylene substrate. The maximum stretching along the field lines corresponds to the case of pure epoxy hardener as illustrated in Fig. 9(a). The rim contour of the expanding drop in Fig. 9(a) reveals some distortions in the field direction. The stretching results in a few fingerlike dendritic structures developing at the drop contact line as it approaches the electrodes. The panels in Fig. 9 allow one to grasp the significant electrohydrodynamic effects in cases of a pure epoxy hardener and mixed epoxy resin and hardener. The drop of epoxy resin and hardener also experienced significant stretching at the same electric field of 10 kV [Fig. 9(b)], albeit not to that extent as with the less viscous pure epoxy hardener [Fig. 9(a)]. The slightly diminished stretching of the epoxy resin and hardener drops in comparison with those with epoxy hardener alone is caused by a higher viscous dissipation in the former case. Moreover, the electric field stretches the drops in such a way that the wetted area covered at time moment $t = 16$ s increases compared to that in the case at 0 kV for both fluids. For incompressible liquids, this means that the liquid layer becomes thinner under the action of the applied voltage in comparison to the case without the electric field. Moreover, electrowetting associated with the additional electrostatic energy at the drop footprint also affects the dynamics of spreading and stretching of drops of pure hardener and epoxy resin and hardener (Chen and Bonaccurso, 2014; Mugele and Baret, 2005; Mugele and Heikenfeld, 2019; and Yarin, 2020).

The traces of drop footprints in the case of silicone oil at the applied voltages of 0, 7, and 10 kV are combined in Fig. 10. The superimposed contours reveal that there is no visible drop stretching due to the applied electric field, but rather, the drop wetted areas are purely wettability-driven on the porous material following the grooves' orientation (the x axis).

It should be emphasized that the wetted areas for drops of silicone oil illustrated in Fig. 10 are very close to each other after 1 s with or without electric field applied. Accordingly, one can conclude that the footprint spreading illustrated in Fig. 10 is purely wettability-driven up to 7 s after the drop impact (the entire period covered in Fig. 10). The contour traces only slightly differ with each other because of the effect of the individual features of each balsa specimen used in each trial. Therefore, the macro- and micro-structure of each balsa specimen (e.g., their groove pattern) play some role in the wettability-driven spreading, accompanied by partial imbibition of silicone oil into pores. Microstructural features (such as grooves) in balsa wood depend on multiple factors, such as the habitat and age of the tree, its cellular structure, the existence of sap channels and ray cells, and how uniform is the distribution in type and size of cells throughout its grain cross section (Vural and Ravichandran, 2003). The size of the balsa grooves (the groove length and diameter) facilitates the wettability-driven impregnation of liquid in the porous substrate. This is, probably, because the leading edge of a liquid tongue in the pore becomes convex, which diminishes local pressure there, and thus, facilitates imbibition. On the other hand, plastic surfaces, such as polypropylene, are thermally processed and extruded, which helps to control their surface roughness and, in particular, to prevent formation of any grooves.

The drop contour traces observed in the experiments with turpentine oil with golden yellow oak and black aniline dyes on balsa wood substrates are presented in Fig. 11. The superposition of the footprint areas captured in the experiments (Figs. 6 and 7) at the time moments $t = 4$ ms and $t = 0.5$ s elucidates the drop wetted areas at 0 kV and at the highest voltage of 10 kV corresponding to the electric field strength of 6.6×10^5 V/m.

It should be emphasized that the experiments were repeatable in multiple trials for each dielectric substrate (porous and non-porous) without and with the applied electric field, and the cumulative data displayed in Figs. 2–11 are representative of all the trials conducted. The contours captured in the top views in Figs. 8–11 encompass the footprint areas listed in Table III. The average area increase with voltage observed in Table III demonstrates the effect of the applied in-plane electric field on drop stretching and wettability-driven spreading for each fluid on the corresponding dielectric substrate.

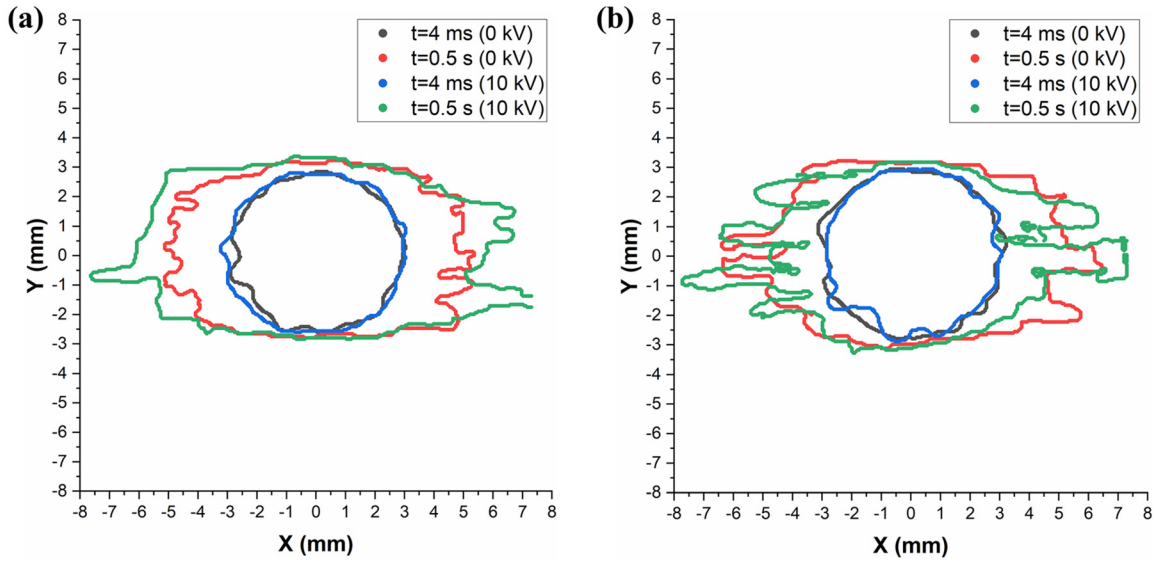

FIG. 11. Footprint area contours of drops of turpentine oil mixed with oil-soluble aniline dyes on balsa wood substrates without and with the electric field acting after impact experimentally observed in the top view: (a) golden yellow oak dye at 7 wt. % concentration and (b) black dye at 10 wt. % concentration. The left-hand side electrode is the anode, and the right-hand side one is grounded (the cathode). The Cartesian coordinates on the substrates are denoted as x (in the field direction) and y.

The data listed in Table III reveal a remarkable effect of the electric field for all the fluids studied, except silicone oil on balsa wood, which confirms the findings of the present group in Granda *et al.* (2022a). On the other hand, drops of turpentine oil with aniline dyes on balsa wood substrate reveal only a slight effect of the in-plane electric field on drop spreading on the porous substrate at a high voltage of 10 kV. Here, wettability-driven spreading accompanied by imbibition is the main mechanism during the advancing motion of the drops after impact. Table III illustrates that higher electric field strengths result in a more pronounced increase in the wetted area for polypropylene substrate (for all the fluids used in the experiments with such a substrate). Similarly, epoxy resin on porous balsa wood revealed a significant increase in the final footprint area on polypropylene, which indicates that applications of the in-plane DC voltages in painting and coating hold great promise. However, silicone oil spreading is practically unaffected even by strong electric fields because of an insufficient ionic concentration. It should be noted that the negative sign in the percentage change of the wetted area of silicone oil on balsa in Table III means that the average of all the trials at 0 and 10 kV at the end of each high-speed recording ($t = 7$ s) revealed a tiny decrease, which does not imply any effect of the applied voltage, but rather, an effect of the texture and macrostructure of porous balsa on drop spreading.

Furthermore, the dependences on time of the effective radius of drops of epoxy resin and silicone oil on balsa wood without and with the electric field are presented in Fig. 12. Note that the data points in Fig. 12 represent the average of all the trials conducted for each fluid at the applied voltages of 0 and 10 kV.

Note also that the data points depicting the drop radius before impact correspond to a slightly negative t, because they were recorded for drops in flight. Additionally, it should be mentioned that the red

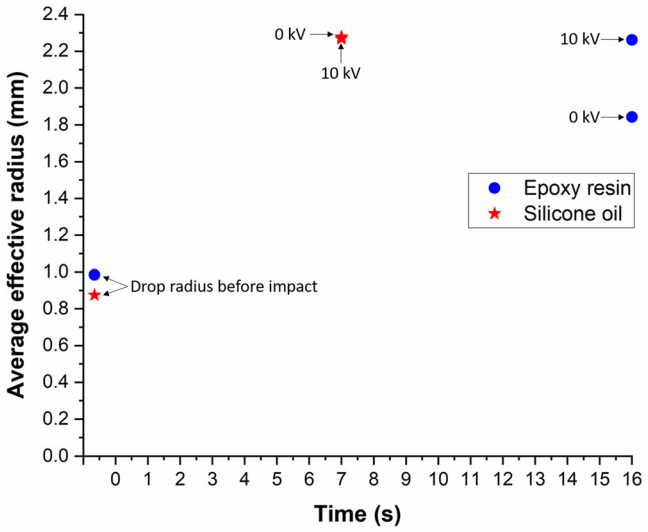

FIG. 12. Average effective radius of drops of epoxy resin and silicone oil on balsa wood substrate without and with the electric field after impact measured as a function of time. The drop radii before impact are also shown. The data points at 0 and 10 kV correspond to the end of the high-speed recording after drop impact ($\sim t = 16$ s for epoxy resin and $\sim t = 7$ s for silicone oil).

data points for silicone oil without and with the applied voltage overlap with each other at $t = 7$ s because the application of the electric field did not have any effect on the final wetted area in this case in Fig. 12 and Table III. On the other hand, the applied voltage of 10 kV clearly had a significant effect on epoxy resin drops after impact on porous balsa as seen from the data for $t = 16$ s.

IV. CONCLUSION

The spreading of drops impacting onto balsa wood and polypropylene substrates, without and with the effect of the electric field, has been explored in the present study. Drop impacts of epoxy resin, epoxy hardener, epoxy resin and hardener, silicone oil, and turpentine oil with oil-soluble aniline dyes were experimentally investigated using the porous and nonporous substrates (balsa wood and polypropylene, respectively) at the applied voltages of 0, 7, and 10 kV. The experiments revealed that the electric field can significantly stretch drops of epoxy resin, epoxy hardener, and epoxy resin and hardener after impact on polypropylene substrate. Furthermore, the experimental observations with turpentine oil suspensions of dye particles demonstrated a weaker effect of the applied voltages of 7 and 10 kV on drops impacting onto balsa wood. Here, diffusion-like spreading and wettability-driven imbibition became the dominant mechanisms.

The high-speed recordings demonstrated a slight effect of the applied electric field of 10 kV (corresponding to the electric field strength of 6.6×10^5 V/m) on drops of epoxy resin after impact onto porous balsa wood. In this case, the experimental observations also revealed wettability-driven spreading in the cases without the electric field applied and at the applied voltage of 10 kV. In the latter case, the wettability-driven spreading was slightly enhanced by the electric field. Due to the presence of the electric field, the drop footprint area increased by $8.5 \pm 0.4\%$ and $3.9 \pm 0.9\%$ for turpentine oil with golden yellow and black aniline dyes, respectively, 0.5 s after impact on balsa wood; $50.5 \pm 3.8\%$ for epoxy resin, 16 s after impact onto balsa wood; and by $95.1 \pm 1.7\%$, $105.3 \pm 16.7\%$, and $74.3 \pm 6.9\%$ for epoxy resin, epoxy hardener, and epoxy resin and hardener, respectively, on polypropylene substrate.

Furthermore, it was experimentally shown that individual drops of silicone oil after impact onto the porous balsa substrate subjected to the electric field strengths of 4.6×10^5 and 6.6×10^5 V/m corresponding to the applied voltages of 7 and 10 kV, respectively, were practically unaffected by the electric field presumably because pure silicone oil used in the present experiments does not possess enough preexisting ions and counterions and thus does not support any significant Maxwell stresses at the surface available for drop stretching. This conclusion is also confirmed by the dependence on time of the area-effective radius of drops of silicone oil on balsa without and with the electric field of 10 kV. Silicone oil spreading on balsa wood was driven by wettability and guided by grooves in the inter-electrode direction, as the observations in the 0–7 s interval revealed.

ACKNOWLEDGMENTS

The authors acknowledge the financial support from the National Science Foundation through Award No. 2312197.

AUTHOR DECLARATIONS

Conflict of Interest

The authors have no conflicts to disclose.

Author Contributions

Rafael Granda: Conceptualization (equal); Formal analysis (equal); Investigation (equal); Methodology (equal); Writing – original draft (equal); Writing – review & editing (equal). **Vitaliy Yurkiv:** Funding acquisition (equal); Investigation (equal); Methodology (equal); Writing – review & editing (equal). **Farzad Mashayek:** Funding acquisition (equal); Project administration (equal); Resources (equal); Supervision (equal); Writing – review & editing (equal). **Alexander L. Yarin:** Conceptualization (equal); Funding acquisition (equal); Project administration (equal); Supervision (equal); Writing – review & editing (equal).

DATA AVAILABILITY

The data that support the findings of this study are available from the corresponding author upon reasonable request.

REFERENCES

Alia-Syahirah, Y., Paridah, M. T., Hamdan, H., Anwar, U. M. K., Nordahlia, A. S., and Lee, S. H., "Effects of anatomical characteristics and wood density on surface roughness and their relation to surface wettability of hardwood," J. Trop. For. Sci. **31**, 269–277 (2019).

Benkreif, R., Brahmia, F. Z., and Csiha, C., "Influence of moisture content on the contact angle and surface tension measured on birch wood surfaces," Eur. J. Wood Prod. **79**, 907–913 (2021).

Bochkarev, A. A., Geshev, P. I., Polyakova, V. I., and Yavorskii, N. I., "Connection between the deformation of paint droplets during deposition on the surface being painted and the orientation of pigment particles," Theor. Found. Chem. Eng. **45**, 399–408 (2011).

Cai, Y., Wu, J., Wang, K., Dong, Y., Hu, J., Qu, J., Tian, D., Li, J., and Fu, Q., "Thermo-controlled, self-released smart wood tailored by nanotechnology for fast clean-up of highly viscous liquids," SmartMat **4**, e1133 (2023).

Chen, L. and Bonaccurso, E., "Electrowetting—From statics to dynamics," Adv. Colloid Interface Sci. **210**, 2–12 (2014).

Csanády, E., Magoss, E., and Tolvaj, L., *Quality of Machined Wood Surfaces* (Springer International Publishing, Switzerland, 2015).

Frank, X. and Perré, P., "Droplet spreading on a porous surface: A lattice Boltzmann study," Phys. Fluids **24**, 042101 (2012).

Fu, Q., Ansari, F., Zhou, Q., and Berglund, L. A., "Wood nanotechnology for strong, mesoporous, and hydrophobic biocomposites for selective separation of oil/water mixtures," ACS Nano **12**, 2222–2230 (2018).

Fu, Z., Zhou, Y., Gao, X., Liu, H., and Zhou, F., "Changes of water related properties in radiata pine wood due to heat treatment," Constr. Build. Mater. **227**, 116692 (2019).

Granda, R., Li, G., Yurkiv, V., Mashayek, F., and Yarin, A. L., "Dielectrophoretic stretching of drops of silicone oil: Experiments and multi-physical modeling," Phys. Fluids **34**, 042108 (2022a).

Granda, R., Plog, J., Li, G., Yurkiv, V., Mashayek, F., and Yarin, A. L., "Evolution and shape of 2D Stokesian drops under the action of surface tension and electric field: Linear and nonlinear theory and experiment.," Langmuir **37**, 11429–11446 (2021a).

Granda, R., Yurkiv, V., Mashayek, F., and Yarin, A. L., "Metamorphosis of trilobite-like drops on a surface: Electrically driven fingering," Phys. Fluids **33**, 124107 (2021b).

Granda, R., Yurkiv, V., Mashayek, F., and Yarin, A. L., "Paint drop spreading on wood and its enhancement by an in-plane electric field," Phys. Fluids **34**, 122112 (2022b).

Jang, E., Kang, C., and Jang, S., "Pore characterization in cross section of yellow poplar (*Liriodendron tulipifera*) wood," J. Korean Wood Sci. Technol. **47**, 8–20 (2019).

Karniadakis, G., Beskok, A., and Aluru, N., "Microflows and nanoflows," in *Fundamentals and Simulation* (Springer, Berlin, 2005).

Lee, J. B., Derome, D., Guyer, R., and Carmeliet, J., "Modeling the maximum spreading of liquid droplets impacting wetting and nonwetting surfaces," Langmuir **32**, 1299–1308 (2016).

Lee, M. W., Latthe, S. S., Yarin, A. L., and Yoon, S. S., "Dynamic electrowetting-on-dielectric (DEWOD) on unstretched and stretched Teflon," Langmuir **29**, 7758–7767 (2013).

Meng, S., Yang, R., Wu, J. S., and Zhang, H., "Simulation of droplet spreading on porous substrates using smoothed particle hydrodynamics," Int. J. Heat Mass Transfer **77**, 828–833 (2014).

Mikkelsen, A., Khobaib, K., Eriksen, F. K., Måløy, K. J., and Rozynek, Z., "Particle-covered drops in electric fields: Drop deformation and surface particle organization," Soft Matter **14**, 5442–5451 (2018).
Mugele, F. and Baret, J.-C., "Electrowetting: From basics to applications," J. Phys.: Condens. Matter **17**, R705–R774 (2005).
Mugele, F. and Heikenfeld, J., *Electrowetting: Fundamental Principles and Practical Applications* (Wiley-VCH, Weinheim, 2019).
Perré, P., Nguyen, D. M., and Almeida, G., "A macroscopic Washburn approach of liquid imbibition in wood derived from X-ray tomography observations," Sci. Rep. **12**, 1750 (2022).
Plötze, M. and Niemz, P., "Porosity and pore size distribution of different wood types as determined by mercury intrusion porosimetry," Eur. J. Wood Prod. **69**, 649–657 (2011).
Pohl, H. A., *Dielectrophoresis* (Cambridge University Press, Cambridge, 1978).
Sankaran, A., Wu, J., Granda, R., Yurkiv, V., Mashayek, F., and Yarin, A. L., "Drop impact onto polarized dielectric surface for controlled coating," Phys. Fluids **33**, 062101 (2021).
Šoškić, B., Govedar, Z., Todorović, N., and Petrović, D., "Basic physical properties of Spruce wood (Picea abies Karst.) from plantations," Bull. Fac. For. **96**, 97–110 (2007).
Vidiella del Blanco, M., Fischer, E. J., and Cabane, E., "Underwater superoleophobic wood cross sections for efficient oil/water separation," Adv. Mater. Interfaces **4**, 1700584 (2017).
Vural, M. and Ravichandran, G., "Microstructural aspects and modeling of failure in naturally occurring porous composites," Mech. Mater. **35**, 523–536 (2003).
Wang, W., Zhu, Y., Cao, J., and Sun, W., "Correlation between dynamic wetting behavior and chemical components of thermally modified wood," Appl. Surf. Sci. **324**, 332–338 (2015).
Wood–Densities of Various Species, see www.engineeringToolBox.com for "The Engineering Toolbox" (2001).
Yarin, A. L., "Wetting for self-healing, and electrowetting for additive manufacturing," Curr. Opin. Colloid Interface Sci. **51**, 101378 (2020).
Yarin, A. L., Lee, M. W., An, S., and Yoon, S. S., *Self-Healing Nanotextured Vascular Engineering Materials* (Springer Nature, Cham, Switzerland, 2019).
Yarin, A. L., Pourdeyhimi, B., and Ramakrishna, S., *Fundamentals and Applications of Micro- and Nanofibers* (Cambridge University Press, Cambridge, 2014).
Yarin, A. L., Roisman, I. V., and Tropea, C., *Collision Phenomena in Liquids and Solids* (Cambridge University Press, Cambridge, 2017).
Yurkiv, V., Yarin, A. L., and Mashayek, F., "Modeling of droplet impact onto polarized and nonpolarized dielectric surfaces," Langmuir **34**, 10169–10180 (2018).
Zhou, M., Caré, S., Courtier-Murias, D., Faure, P., Rodts, S., and Coussot, P., "Magnetic resonance imaging evidences of the impact of water sorption on hardwood capillary imbibition dynamics," Wood Sci. Technol. **52**, 929–955 (2018).